Optical Materials 34 (2012) 1277–1281

Contents lists available at SciVerse ScienceDirect

Optical Materials

journal homepage: www.elsevier.com/locate/optmat

Defect modes in optically induced photonic lattices in biased photovoltaic–photorefractive crystals

Keqing Lu [a,*], Jianbang Guo [b], Kehao Li [b], Weijun Chen [a], Tongtong Sun [a], Fengxue Yao [a], Pingjuan Niu [a], Jingjun Xu [c]

[a] School of Electronics and Information Engineering, Tianjin Polytechnic University, Tianjin 300387, China
[b] State Key Laboratory of Transient Optics and Photonics, Xi'an Institute of Optics and Precision Mechanics, Chinese Academic of Sciences, Xi'an 710119, China
[c] Department of Physics, Nankai University, Tianjin 300071, China

ARTICLE INFO

Article history:
Received 19 December 2011
Received in revised form 28 January 2012
Accepted 28 January 2012
Available online 2 March 2012

Keywords:
Defect solitons
Photonic lattices
Photorefractive effect
Non-linear optics

ABSTRACT

We show that defect modes in optically induced photonic lattices are possible in biased photovoltaic–photorefractive crystals. These defect modes exist in different bandgaps when the defect strength is changed. When the defect strength is positive, there is a defect-mode branch in each bandgap. When the defect strength is negative, there is a defect-mode branch in the first bandgap and are many defect-mode branches in higher bandgaps. For a given defect strength, the strongest confinement of the defect modes appears in the semi-infinite bandgap when the defect strength is positive and in the first bandgap when the defect strength is negative. On the other hand, these defect modes are those studied previously in optically induced photonic lattices in biased non-photovoltaic–photorefractive crystals when the bulk photovoltaic effect is negligible and predict those in optically induced photonic lattices in photovoltaic–photorefractive crystals when the external bias field is absent.

Light propagation has been widely researched in periodic photonic lattices because of its physics and light-routing applications. At present, a wide variety of solitons in uniformly periodic photonic lattices are known: fundamental solitons [1–7], dipole solitons [8,9], vortex solitons [10–14], reduced-symmetry solitons [15], embedded-soliton trains [16], and so on—many of which have been experimentally observed. In uniformly periodic photonic lattices, a new feature is the existence of bandgaps inside Bloch bands, where linear light propagation is forbidden because of the repeated Bragg reflections. To guide light in periodic media, one of the convenient ways is to introduce a defect into the periodic medium. Such a defect can support defect modes in bandgaps of the periodic medium. Defects and the corresponding defect modes have been investigated in photonic crystals [17]. In photorefractive crystals, optically induced reconfigurable photonic lattices with and without defects have been successfully generated [2,6,18]. Defect modes in one-dimensional (1D) photonic lattices were the first to have been proposed [19,20] and observed [21]. Defect solitons in 1D photonic lattices have been theoretically analyzed [22]. In 2D photonic lattices, defect modes [23] and defect solitons [24] have also been predicted. However, these studies focused on optically induced photonic lattices in biased non-photovoltaic–photorefractive crystals. Therefore, it is interesting to know whether optically induced photonic lattices can support defect modes in photovoltaic–photorefractive crystals with and without the external bias field.

In this paper, we report on that defect modes in optically induced photonic lattices in biased photovoltaic–photorefractive crystals can exist in different bandgaps when the defect strength is changed. We show that for a positive defect, there is a defect-mode branch in each bandgap and that for a negative defect, there is a defect-mode branch in the first bandgap and are many defect-mode branches in higher bandgaps. We find that for a given defect strength, the strongest confinement of the defect modes appears in the semi-infinite bandgap when the defect strength is positive and in the first bandgap when the defect strength is negative. When the bulk photovoltaic effect is negligible, these defect modes are those studied previously in optically induced photonic lattices in biased non-photovoltaic–photorefractive crystals. When the external bias field is absent, these defect modes predict those in optically induced photonic lattices in photovoltaic–photorefractive crystals.

To start, let us consider an ordinarily polarized lattice beam with a single-site defect that propagates in a photovoltaic–photorefractive crystal along the *z* axis and is allowed to diffract only along the *x* direction. For demonstration purposes, let the photovoltaic–photorefractive crystal be $LiNbO_3$ with its optical *c* axis oriented along the *x* direction. Moreover, let us assume that an extraordinarily polarized probe beam with a very low intensity is launched into the defect site and that the external bias electric field

* Corresponding author.
E-mail address: kqlutj@126.com (K. Lu).

0925-3467/$ - see front matter Crown Copyright © 2012 Published by Elsevier B.V. All rights reserved.
doi:10.1016/j.optmat.2012.01.036

is applied in the x direction (i.e., the c axis). This probe beam is incoherent with the lattice beam and propagates collinearly with it. Under these conditions, the perturbed extraordinary refractive index along the x axis is given by $n_e'^2 = n_e^2 - n_e^4 r_{33} E_{sc}$, where n_e is the unperturbed extraordinary index of refraction, r_{33} is the electro-optic coefficient, $\mathbf{E}_{sc} = \mathbf{i}E_{sc}$ is the induced space-charge electric field, and $\mathbf{i}$ is the unit vector pointing to the c-axis direction. The electric-field component E of the probe beam is then expressed as usual in terms of slowly varying envelope $\phi(x, z)$, that is $E = \phi(x, z)\exp(ik_1 z)$, where $k_1 = k_0 n_e$, $k_0 = 2\pi/\lambda_0$ is the wave number, and λ_0 is the free-space wavelength of the lightwave employed. At this point, the power density profile of the probe beam, $I(x, z)$, can be also expressed in terms of the envelope $\phi(x, z)$ by use of Poynting's theorem, i.e., $I = (n_e/2\eta_0)|\phi|^2$, where η_0 represents the free-space intrinsic impedance. By employing standard procedures, we readily obtain the following paraxial equation of diffraction [25]

$$i2k_1\frac{\partial\phi}{\partial z} + \frac{\partial^2\phi}{\partial x^2} - k_0^2(n_e^4 r_{33} E_{sc})\phi = 0. \tag{1}$$

Under steady-state conditions, the induced space-charge electric field E_{sc} can be obtained from the Kukhtarev–Vinetskii model and it is approximately given by [26]

$$E_{sc} = E_0'\frac{I_d}{I_L' + I_d} - E_p'\frac{I_L'}{I_L' + I_d}. \tag{2}$$

In the above equation, we have assumed that the probe beam is a very low intensity. Moreover, the constant field E_0' can be obtained from the potential condition $\oint \mathbf{E}_{sc}\cdot d\mathbf{l} = 0$, E_p' is the photovoltaic field constant, and I_d is the dark irradiance of the crystal. $I_L' = I_0'\cos^2 x[1 + \delta f_D(x)]$ is the intensity function of the photovoltaic–photorefractive lattice, where I_0' is the peak intensity of the otherwise uniform photonic lattice (i.e., far away from the defect site), $f_D(x)$ is a localized function describing the shape of the defect, and δ controls the strength of the defect. For a positive defect $\delta > 0$, the lattice light intensity I_L' at the defect site is higher than that at the surrounding sites. For a negative defect $\delta < 0$, the lattice intensity I_L' at the defect site is lower than that at the surrounding sites. When $\delta = -0.75$, the corresponding lattice intensity profile is displayed in Fig. 8s. For convenience, let us adopt the following dimensionless variables and coordinates, i.e., let $Z = z/(2k_1T^2/\pi^2)$, $X = x/(T/\pi)$, and $\phi = (2\eta_0 I_d/n_e)^{1/2}U$, where T is the lattice spacing. By employing these latter transformations and by substituting Eq. (2) into Eq. (1), the nondimensionalized model equation is found to satisfy:

$$i\frac{\partial U}{\partial Z} + \frac{\partial^2 U}{\partial X^2} - \frac{E_0}{1 + I_L}U + E_p\frac{I_L}{1 + I_L}U = 0, \tag{3}$$

where

$$I_L = I_0\cos^2 X\{1 + \delta f_D(X)\}, \tag{4}$$

$E_0 = E_0'/(\pi^2/T^2k_0^2n_e^4r_{33})$, $E_p = E_p'/(\pi^2/T^2k_0^2n_e^4r_{33})$, and $I_0 = I_0'/I_d$. In this paper, let us assume that $f_D(X) = \exp(-X^8/128)$, which shows that the defect is restricted to a single lattice site at $X = 0$. Notice that other choices of single-site defect functions $f_D(X)$ give similar results. Moreover, we consider the following examples: Let $\lambda_0 = 0.5$ µm, $T = 20$ µm, and $I_0 = 3$. The $LiNbO_3$ parameters are taken here to be $n_e = 2.2$, $r_{33} = 30\times10^{-12}$ m/V, and $E_p' = 40$ kV/cm. For this set of values, $E_p \approx 18$, one X unit corresponds to 6.4 µm, one Z unit corresponds to 2.2 mm, and one E_0 unit corresponds to 222 V/mm. The second term of Eq. (3) describes the diffraction spreading of the probe beam. The third and fourth terms describe the influence of drift and photovoltaic effect of the photorefractive nonlinearity, respectively. The third term supports defect modes studied previously in optically induced photonic lattices in biased non-photovoltaic–photorefractive crystals [19,20], whereas the fourth term supports defect modes in optically induced photonic lattices in photovoltaic–photorefractive crystals, which will be demonstrated in what follows. The value of E_0 is associated with the applied external electric field.

In order to analyze defect modes in the bandgaps, let us first understand the dispersion relation and bandgap structure of Eq. (3) with $\delta = 0$. According to the Bloch theorem, eigenfunctions of Eq. (3) with $\delta = 0$ can be sought in the form of $U(X, Z) = u(X)\exp[ikX - i\beta Z]$, where k is wave number in the first Brillouin zone bounded between $-1 \leqslant k \leqslant 1$, β is the diffraction relation, $u(X)$ is a periodic function with the same period π (in normalized units) as the potential term I_L with $\delta = 0$. Substitution of this latter form of $U(X, Z)$ into Eq. (3) with $\delta = 0$ yields

$$\frac{\partial^2 u}{\partial X^2} + 2ik\frac{\partial u}{\partial X} - k^2U - V(X)U = -\mu U, \tag{5}$$

where

$$V(X) = \frac{E_0}{1 + I_0\cos^2(X)} - \frac{E_pI_0\cos^2(X)}{1 + I_0\cos^2(X)}. \tag{6}$$

Eq. (5) gives the dispersion relation, which contains an infinite number of branches in the first Brillouin zone. Each branch corresponds to a Bloch band. The gaps between adjacent branches are the bandgaps. Fig. 1 depicts the dispersion relation of a uniform lattice at $E_0 = 12$, $E_p = 18$, and $I_0 = 3$. It reveals that there exist four complete gaps which are named the semi-infinite, first, second, and third gaps, respectively. Fig. 2 illustrates the bandgap structure at various values of E_0 when $E_p = 18$ and $I_0 = 3$. Bloch states on the edges of Bloch bands are important because defect modes bifurcate from such Bloch states, as shown in Fig. 4. On these edges, $k = 0$ or $k = \pm1$. The first six Bloch states at $E_0 = 12$, $E_p = 18$, and $I_0 = 3$ are shown in Fig. 3. Bloch states on the edges of first and third Bloch bands are symmetric, and Bloch states on the edges of second Bloch band are antisymmetric, in X.

We seek the defect modes in Eq. (3) in the form

$$U(X, Z) = u(X)\exp(-i\beta Z), \tag{7}$$

where function $u(X)$ is localized in X and β is a propagation constant lying inside bandgaps of the periodic lattice. Substitution of Eq. (7) into Eq. (3) yields

$$\frac{d^2u}{dX^2} + \left(\beta - \frac{E_0}{1 + I_L} + E_p\frac{I_L}{1 + I_L}\right)u = 0, \tag{8}$$

from which the mode $u(X)$ can be determined by a numerical method. Such a numerical method is to expand the solution $u(X)$ into discrete Fourier series and then convert Eq. (8) into a matrix eigenvalue problem with β as the eigenvalue [20].

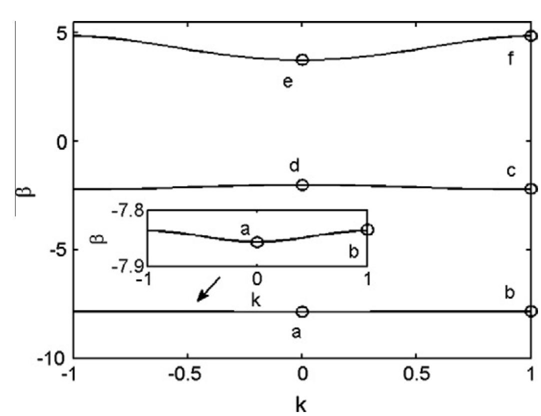

Fig. 1. Dispersion relation of a uniform lattice at $E_0 = 12$, $E_p = 18$, and $I_0 = 3$. Bloch states at circled locations are shown in Fig. 3.